Diel Redox Cycle of Manganese in the Surface Arctic Ocean

Y. Xiang*, P. J. Lam, J. M. Lee

Department of Ocean Sciences, University of California, Santa Cruz, CA 95064 USA

Corresponding author: Yang Xiang (yaxiang@ucsc.edu)

Key Points:

- Particulate manganese oxidation states are more reduced in the day and more oxidized at night in the surface Arctic Ocean;
- The Mn diel cycle results from the conversion between dissolved Mn and particulate Mn(III/IV) oxides regulated by light;
- The length of night and intensity of light exposure are two main controls on the magnitude of particulate Mn average oxidation states.

Abstract

Knowledge of the chemical speciation of particulate manganese (pMn) is important for understanding the biogeochemical cycling of Mn and other particle-reactive elements. Here, we present the synchrotron-based X-ray spectroscopy derived average oxidation state (AOS) of pMn in the surface Arctic Ocean collected during the U.S. GEOTRACES Arctic cruise (GN01) in 2015. We show that the pMn AOS is less than 2.4 when sampled during the day and more than ~3.0 when sampled at night. We hypothesize that an active light-dependent redox cycle between dissolved Mn and particulate Mn(III/IV) exists during the day-night cycle in the surface Arctic Ocean, which occurs on the time scale of hours. The magnitude of observed pMn AOS is likely determined by the net effect of the length of the previous night and integrated light level before the end of pMn sampling.

Plain Language Summary

Manganese (Mn) exists in three oxidation states (II, III, and IV) in the ocean. The difference in oxidation states of Mn minerals leads to differences in their capacities to oxidize and sorb other elements, and thereby affects their role in marine redox and nutrient cycling. In this study, we measured the oxidation states of marine particulate Mn in the surface Arctic Ocean. Our results demonstrate a tight coupling between sunlight and particulate Mn oxidation states: more Mn(II) exists in the daytime, whereas more Mn(III/IV) exists during the night. The light-dark cycle is an important driver in the rapid transition between Mn(II) and Mn(III/IV).

Keywords: Manganese; Photoreduction; Oxidation; Arctic Ocean; Synchrotron X-ray fluorescence (XRF); GEOTRACES

1 Introduction

Manganese (Mn) is the 3rd most abundant transition metal in Earth's crust and exists in three oxidation states (II, III, and IV) in the ocean. Mn is an essential element to life and used to catalyze the oxidation of water to O_2 in Photosystem II (Yano et al., 2006) by phytoplankton, and to detoxify cells from superoxide radicals via the antioxidant enzyme Mn superoxide dismutase (Peers & Price, 2004). Oxidation from dissolved Mn(II) to particulate Mn(III/IV) oxides is known to proceed through two sequential one-electron reactions (Luther, 2005). The final oxidation product, Mn(III/IV) oxide, is a strong natural oxidant and is also known as the "scavenger of the sea" (Goldberg, 1954; Tebo et al., 2004). Although Mn is an important micronutrient for phytoplankton growth, dissolved Mn is often characterized by maximum concentrations at the surface ocean (van Hulten et al., 2017) due to photoreduction of Mn(III/IV) oxides (Sunda & Huntsman, 1987, 1994; Sunda et al., 1983) and is thus not typically limiting, except for in the Southern Ocean (Browning et al., 2021; Middag et al., 2013).

Recent GEOTRACES cruises have demonstrated that the Arctic Ocean is enriched in Mn because of riverine, sedimentary and hydrothermal sources (Charette et al., 2020; Colombo et al., 2020; Jensen et al., 2020; Middag et al., 2011; Xiang & Lam, 2020). The Mn concentration distribution in the Western Arctic Ocean is characterized by surface maxima in the Polar Mixed Layer in the dissolved phase and distinct elevations at halocline depths in the particulate phase (Jensen et al., 2020; Xiang & Lam, 2020). Investigations of Mn cycling in the Arctic Ocean have generally focused on processes spanning time scales of several months to years during transport from shelves to central basins. However, a diel cycle in the concentrations of Mn, in both dissolved and particulate phases, has been observed in the coastal Northwest Atlantic Ocean (Oldham et al., 2020; Sunda & Huntsman, 1990).

Here, we use synchrotron-based X-ray absorption spectroscopy (XAS) to examine the chemical speciation of particulate Mn (pMn) and its relationship with light during the U.S. GEOTRACES Arctic cruise (GN01) in 2015. We take advantage of sampling times that spanned a range of light conditions and relatively constant hydrographic parameters throughout the Polar Mixed Layer to reconstruct a pseudo-diel cycle. This study is one of few that focuses on the oxidation state of pMn in the ocean (Hermans et al., 2019; Lee et al., 2021; Oldham et al., 2021), and the first one in the Arctic Ocean. Lee et al. (2021) showed that changes in pMn speciation in the near- vs. far-field 15˚S East Pacific Rise hydrothermal plume were associated with differences in its scavenging affinity for other trace elements and isotopes. Therefore, insights gained in this work help us understand the diel cycling of Mn and potentially also of other pMn-associated elements in the surface Arctic Ocean.

2 Materials and Methods

2.1 Marine particle sampling and chemical analysis

Marine particles were sampled using dual-flow McLane Research in-situ pumps (WTS-LV) during the U.S. Arctic GEOTRACES cruise (GN01) onboard the U.S. Coast Guard Cutter Healy between 9 August and 11 October 2015 (Figure 1). The day-night cycle varied tremendously over the course of the cruise due to changes in sampling latitude and season, with the length of night ranging from 0 to ~14 hours (Table S1).

Particles (0.8-51 μm) were collected with paired 0.8 μm pore-size polyethersulfone Supor™ filters that were downstream of a 51 μm pore-size polyester pre-filter. The typical time

of pumping in the water column was 3-4 hours. Concentrations of pMn were measured by high-resolution inductively coupled mass spectrometry after total digestion (Xiang & Lam, 2020).

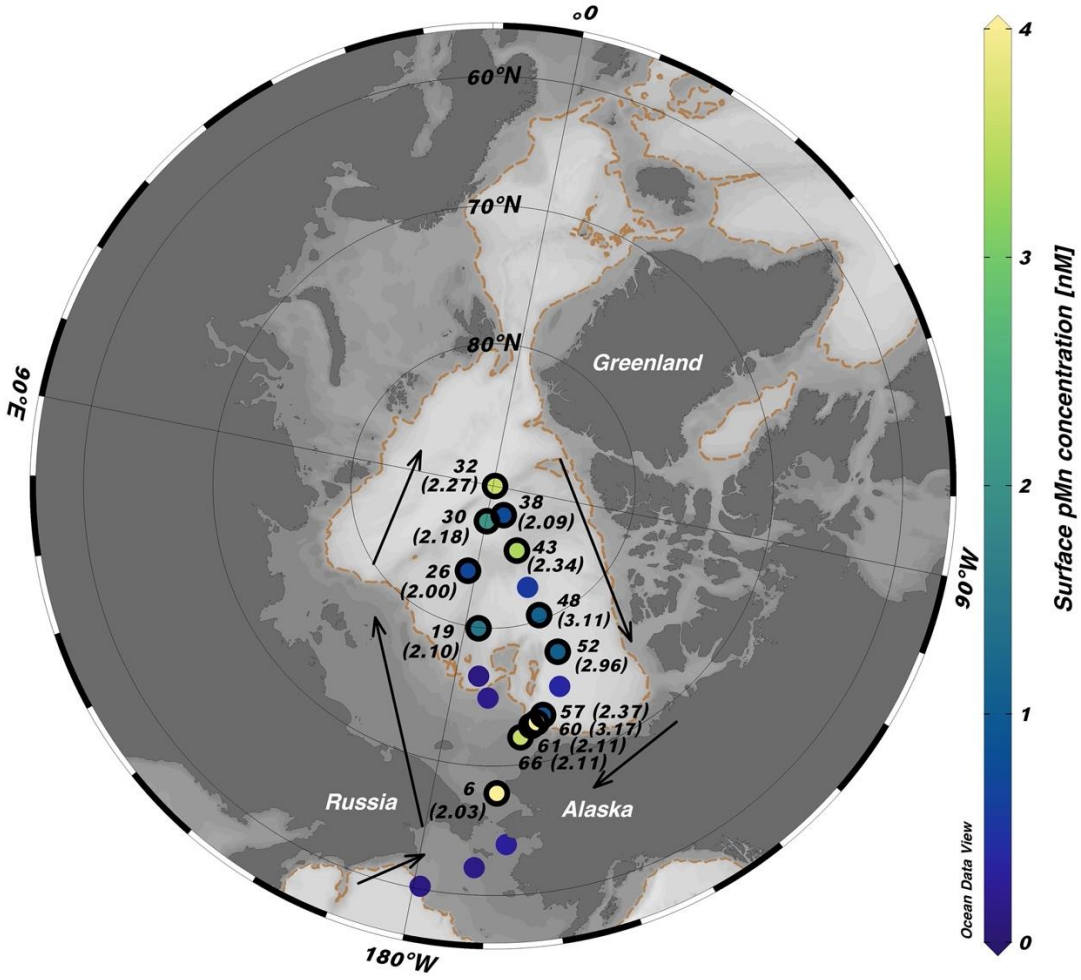

Figure 1. Sampling locations of the GN01 cruise (cruise track: clockwise). Colors show the surface particulate Mn (pMn) concentrations (unit: nmol/L). The ocean bathymetry with 1,000 m contour is indicated as brown dashed lines. Samples analyzed by XANES are outlined by thick black circles and labeled by station numbers. Average oxidation states (AOS) of pMn are labeled next to station numbers within parenthesis.

2.2 Synchrotron X-ray Absorption Spectroscopy (XAS) analysis

Surface samples collected at ~20 m from 13 stations (3 shelf, 1 slope, and 9 basin), together with one sample within the benthic nepheloid layer over the shelf, were analyzed by bulk XAS at the Stanford Synchrotron Radiation Lightsource (SSRL) Beamline 11-2. Prior to exposure to the light source, a subsample of the original filter (usually 1/32 of the whole, equivalent to ~12.5 L of pumped seawater) was rolled into multiple layers to maximize the signal from dilute marine particle samples. The speciation of pMn was determined by X-ray Absorption Near Edge Structure (XANES) spectroscopy using a liquid nitrogen cryostat. Averaged spectra were background removed, normalized and deglitched using the SIXPACK software package (Webb, 2005). No obvious shifts of XANES peaks were observed within 10-20 scans in all samples analyzed, indicating no Mn photoreduction had taken place during analysis (Figure S1). To assess variations in the speciation of pMn in the surface Arctic, we calculated the average oxidation state (AOS) of pMn from linear combination fitting (LCF) of sample XANES spectra in the energy range of 6520-6600 eV using three Mn mineral endmembers to represent three oxidation states of Mn. The Mn(II), Mn(III) and Mn (IV) reference endmembers used are the most reduced pMn among our samples (GT11010s), feitknechtite ($Mn^{III}OOH$), and δ-$Mn^{IV}O_2$, respectively (Text S1). LCF was done using SIXPACK and the goodness of the fits was evaluated by the magnitude of the R-factor (Newville, 2001).

2.3 Environmental parameters

Environmental parameters that can affect Mn redox cycling such as pH, temperature, oxygen, and light levels (Kim et al., 2012; Sunda & Huntsman, 1994; Toyoda & Tebo, 2016; Von Langen et al., 1997) were measured on the Oceanographic Data Facility (ODF) CTD rosette during the cruise (Landing et al., 2017; Woosley et al., 2017). For light levels, photosynthetically

119 available radiation (PAR; wavelength of 400-700 nm) data was collected by a QCP-2300-HP
120 Biospherical PAR sensor. Since shortwave radiation in the UV-A range (wavelength of 350-380
121 nm) is thought to contribute most to reduction of Mn(III/IV) oxides (Sunda & Huntsman, 1994),
122 and since PAR data were collected on different casts than particle samples, the solar zenith angle
123 (SZA), defined as the angle between the sun and the vertical plane, is used to estimate the light
124 level in the surface ocean during particle sampling. The SZA is less than 90˚ when the sun is
125 above the horizon ("daylight"), and greater than 90˚ when the sun is below the horizon ("night").
126 The SZA was calculated with the National Oceanic and Atmospheric Administration Earth
127 Systems Research Laboratory Solar Position Calculator
128 (http://www.esrl.noaa.gov/gmd/grad/solcalc/calcdetails.html) by inputting sampling coordinates
129 and times.

130 PAR values from the ODF CTD are negatively correlated with their corresponding SZA
131 at 20 decibars during the daytime (SZA<90˚), and they are relatively constant and small at night
132 (SZA>90˚) (Figure 2a). The close relationship between PAR and SZA observed during the ODF
133 CTD casts suggests that the magnitude of SZA is a good proxy for visible light levels at 20 m
134 where surface particles were collected, and by extension, possibly for UV-A light as well, given
135 their similar attenuation coefficients (Lee et al., 2013). To account for different weather
136 conditions experienced during the particle sampling at each station, which partly lead to scatter
137 in the relationship between PAR and SZA, we also use underway shortwave radiation
138 (wavelength of ~0.3-3 μm) data measured using a pyranometer above the sea surface at the
139 helicopter deck. Note that underway shortwave radiation data cannot account for variable light
140 attenuation by either ice cover (Stations 19-46: permanent ice cover) or particles in the water
141 column.

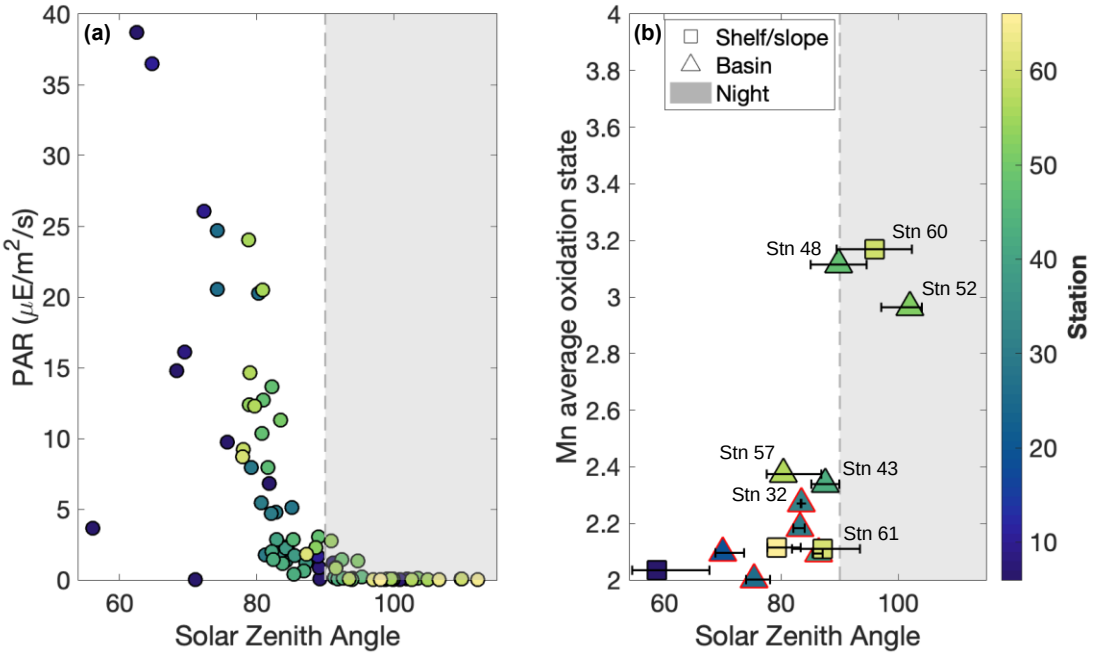

Figure 2. The relationships between solar zenith angle (SZA) and photosynthetically available radiation (PAR) measured in the ODF CTD casts at pressure = 20 decibars (a), and between SZA and Mn average oxidation states (AOS) measured on particles collected in the pump casts at ~20 m (b). The symbols in (b) are the SZA at mid-cast and error bars demonstrate the minimum and maximum SZA during particle sampling. Samples collected under 24-h light conditions are outlined in red.

3 Results and Discussion

3.1 Surface particulate Mn (pMn) speciation

The surface Arctic has median (range) pMn concentrations of 1.0 (0.1-18.7) nmol/L (Figure 1 & Table S1). Surface samples with relatively high pMn concentrations were analyzed

by XANES. The XANES spectra show a pronounced maximum x-ray absorption peak either at 6561 eV or 6551 eV (Figure 3) which indicates oxidized and reduced pMn, respectively. It is worth noting that oxidized pMn samples (Stations 48, 52, 60) also have a shoulder peak at 6551 eV, reflecting the existence of reduced Mn.

Two distinct x-ray absorption peaks at 6552 and 6557.5 eV occur in the benthic nepheloid layer (BNL) sample (Figure S2). Similar XANES spectra have been observed in estuarine sediments in San Francisco Bay (Carroll et al., 2002) and Baltic Sea sediments (Lenz et al., 2014), potentially suggesting a detrital pool of Mn aluminosilicates. We used the BNL XANES as a likely aluminosilicate reference to fit all surface Arctic samples and found that the aluminosilicate signal is only present at shelf Station 6. The surface sample at Station 6 is dominated by the putative Mn aluminosilicates, with the BNL fraction accounting for 68.1% of the XANES signal (Figure S2), suggesting strong sediment resuspension on the Chukchi Shelf (Xiang & Lam, 2020). To compare the non-aluminosilicate fraction to other surface samples, the BNL fraction was removed from the bulk XANES spectrum, and the residual was renormalized. The BNL-corrected sample at Station 6 has a maximum absorption peak at 6551 eV, like the other reduced pMn (Figure 3a).

The pMn AOS estimated from XANES spectra range from 2.00 to 3.17 (Figure 1 & Table S1). More samples (10 out of 13) were characterized by reduced pMn (AOS<2.9) than oxidized pMn. The most oxidized surface pMn (Station 60; AOS=3.17) was best fit when the Mn(IV) reference (δ-$Mn^{IV}O_2$) was included in the fits (Figure S3). For context, the most oxidized pMn AOS below the surface within the dark Pacific-derived halocline (Station 14) has an AOS of 3.65 (Figure S4).

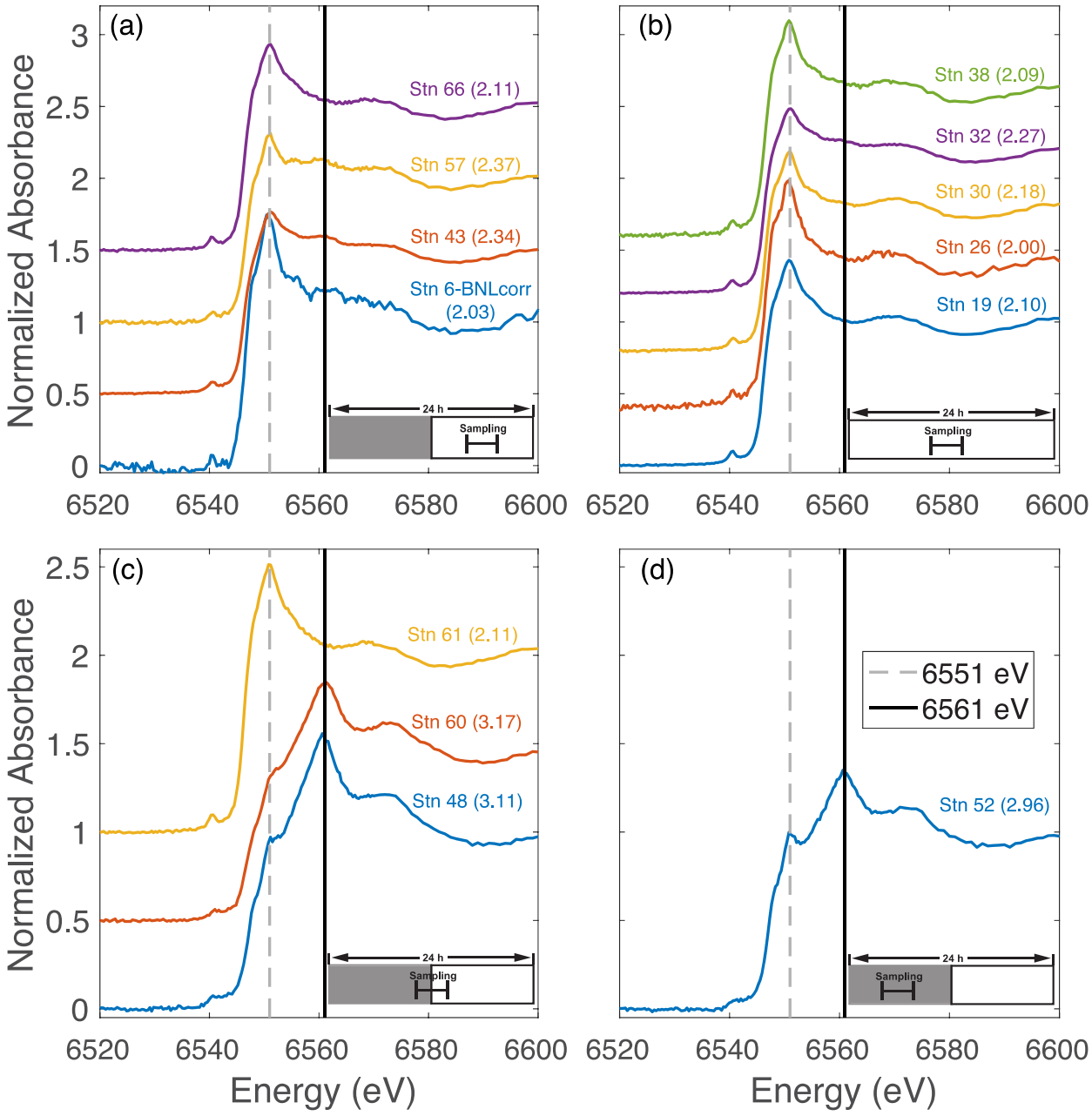

177

178 **Figure 3**. Mn K-edge bulk X-ray absorption near edge structure (XANES) spectra of surface
179 pMn analyzed, grouped by different light levels experienced during the sampling and/or on a
180 daily basis. The selection criteria for four groups are displayed as a cartoon in the bottom right
181 corner of each subplot, illustrating whether there was a day-night cycle at that station during
182 sampling (white-shaded rectangle) and the light level during sampling (horizontal bar). (a):

sampling entirely in the light but experiencing a day-night cycle; (b): sampling entirely in the light and experiencing 24-h light; (c): sampling partially in the light; (d): sampling entirely in the dark but experiencing a day-night cycle. The pMn AOS for each spectrum is labeled next to station numbers within parenthesis.

3.2 Effect of light on pMn speciation

We separate XANES spectra into four groups based on the light level experienced during the 4-hour in-situ sampling and the day-night cycle characterizing that station. The first group experienced full light during sampling, even if a day-night cycle was present at that station (Stations 6, 43, 57, and 66); pMn is generally reduced in this group (Figure 3a). Samples from Stations 43 and 57 also show small peaks at 6561 eV, indicating some presence of oxidized Mn. The second group comprises all surface samples at stations experiencing 24-hour light (Stations 19-38); these spectra exhibit a steep absorption peak at 6551 eV, characteristic of reduced Mn (Figure 3b). A small peak at 6560 eV observed at Station 32 is associated with a high Mn(III) fraction of 19.1% and little Mn(IV) (Table S1). Station 32, within the fast-flowing Transpolar Drift, is characterized by the shortest transport time from the shelf (~6 months) among all surface stations (Kipp et al., 2018). Thus, it may have received shelf-derived particulate Mn(III/IV) that was transported laterally. The third group of samples were collected in partial darkness and are characterized by reduced Mn (Station 61) or a mixture of reduced and oxidized Mn (Stations 48 and 60) (Figure 3c). The fourth group, comprising only one sample (Station 52), was collected in complete darkness. Similar to the more oxidized samples at Stations 48 and 60, pMn at Station 52 is characterized by a mixture of reduced and oxidized Mn (Figure 3d).

To further describe the relationship between pMn speciation and light, we plot the AOS of pMn against the SZA (Figure 2b). We find that pMn is more oxidized when samples were taken at night (SZA>90˚), whereas it is more reduced when sampled during the day (SZA<90˚). Other environmental parameters, e.g., temperature, dissolved oxygen, and pH, that are known to influence Mn oxidation (Toyoda & Tebo, 2016; Von Langen et al., 1997) and reduction (Kim et al., 2012; Sunda & Huntsman, 1994) kinetics, do not have clear correlations with pMn AOS in the surface Arctic during our cruise (Figure S5). Therefore, light levels appear to be the first-order control for pMn AOS in the surface Western Arctic.

3.3 Different pMn phases in the surface Arctic

Diel variations in the redox cycling of Mn have been observed in the coastal Northwest Atlantic Ocean (Oldham et al., 2020; Sunda & Huntsman, 1990). Although our data were not conducted at a single location over a 24-hour period, we treat our dataset as a pseudo-diel study and hypothesize that the high pMn AOS in the dark reflects the oxidation of dissolved Mn into Mn(III/IV) oxides at night (Sunda & Huntsman, 1990), and reduced AOS in the light results from the light-dependent reduction of Mn(III/IV) oxides during the day (Sunda & Huntsman, 1988, 1994; Sunda et al., 1983). Photo-enhanced Mn(II) oxidation in the light mediated by reactions with reactive oxygen species has been reported in other environments and laboratory settings (Hansel & Francis, 2006; Learman et al., 2011; Nico et al., 2002). The lower AOS that we observed during the day suggests that light-dependent reduction is more important than photo-enhanced oxidation in the surface Arctic.

In Sunda and Huntsman (1990)'s study of diel Mn cycling, it was the ascorbate reducible fraction of pMn, i.e., Mn(III/IV) oxides, that exhibited a diel pattern, whereas the ascorbate-resistant pMn remained relatively constant throughout the sampling period. The ascorbate-

resistant pMn likely consists of lithogenic Mn silicates and/or other forms of pMn(II), such as organically bound Mn(II) and adsorbed Mn(II).

In the surface of the Western Arctic, both lithogenic Mn silicates and adsorbed Mn(II) are unlikely to be important components of surface pMn, given their low abundance (cf., Xiang & Lam, 2020) and different spectra shapes (Figure S6 & Table S2), respectively. We hypothesize that the pMn(II) observed in the surface Arctic Ocean, accounting for a median (range) of 86.2% (23.7-100.0%) of total pMn, is likely in the form of a strong organically complexed Mn(II) that is incorporated by phytoplankton. The identity of this organically bound Mn(II) is yet unknown. Model organic Mn compounds such as Mn(II)-citrate, Mn(II)-EDTA, Mn superoxide dismutase (SOD), or Mn(II)-siderophores are characterized by maximum absorption peaks at higher energies than what we observed in the samples (Figure S6 & Table S2) (Blamey et al., 2018; Gunter et al., 2006; Harrington et al., 2012; Machado et al., 2019).

We envision a conceptual model with a base level of organically bound pMn(II) that remains relatively constant through the day and night. At night, oxidation of ambient dissolved Mn adds pMn(III/IV) to the pMn pool. The fraction of pMn(III/IV) that remains suspended in the euphotic zone is completely reduced and returns to the dissolved Mn pool during daytime. The total pMn concentrations and fractions of Mn(III)+Mn(IV) for oxidized samples collected in the dark from Stations 52 and 60 are 1.1 nM and 64.0%, and 18.7 nM and 76.3%, respectively (Table S1). Assuming all particulate Mn(III/IV) is derived from nightly oxidation of dissolved Mn, we calculate that particulate Mn(III/IV) concentrations are 0.7 nM at Station 52 and 14.3 nM at Station 60. For simplicity, if we further assume that oxidation starts at dusk and loss of pMn by sinking is small, net Mn oxidation rates can be estimated by dividing the concentration of oxidized Mn by the length of darkness experienced from dusk to the end of sampling at each

station (Stations 52 and 60: 6.2 and 2.9 hrs, respectively). Our estimated net Mn oxidation rates at Stations 52 and 60 are 0.11 and 4.9 nM/h, respectively. The much slower apparent oxidation rate at basin Station 52 might be explained by colder temperatures in the basin (~-1.5 °C) compared to 0 °C at Station 60 at the shelf/slope, lower dissolved Mn concentrations (Jensen et al., 2020), and/or by different microbial communities (e.g., Lee et al., 2019) affecting the rates of oxidation. These average rates integrating over 6.2 and 2.9 hours are probably lower than the maximum oxidation rate in the surface Arctic but are generally comparable with other reported microbially mediated Mn oxidation rates of 0.1-50 nM/h in marine environments (Clement et al., 2009; Dick et al., 2009; Sunda & Huntsman, 1990).

3.4 Examination of controls on AOS in the surface Arctic

To examine the controls on the magnitude of pMn AOS, we use the length of night from the SZA data to estimate the extent of oxidation, and calculate the integrated shortwave radiation from dawn to the end of particle sampling for each station to estimate the extent of light-dependent reduction (Table S1). We consider shelf/slope and basin stations separately, since they have very different temperatures (Figure S5), nutrient levels, and light attenuation.

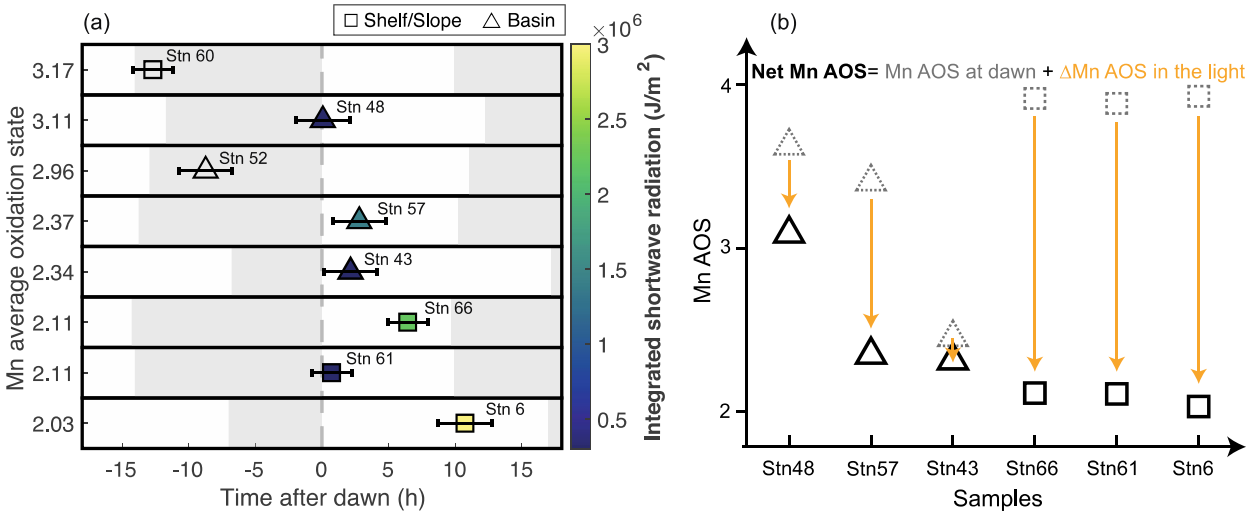

Figure 4. The relationship between time after dawn (unit: hour) and pMn average oxidation state (AOS) (a), and a schematic diagram of AOS during the day-night cycle (b). Shelf/slope and basin stations are marked as squares and triangles respectively. In panel (a), the length of night is indicated by the shaded rectangle for each station and the color bar is the integrated shortwave radiation (unit: J/m^2) from dawn to the end of particle sampling. The black solid symbols in (b) are the net pMn AOS measured by XANES, whereas grey dashed symbols are estimated AOS maxima at dawn (AOS_{dawn}) calculated based on the length of night and Mn oxidation rates (section 3.4).

Both the length of night and intensity of light exposure after dawn influence the measured pMn AOS at the time of sampling: a longer period of darkness results in higher AOS at dawn, whereas higher integrated shortwave radiation decreases AOS in the light (Figure 4). We assume that all basin and shelf/slope stations have net Mn oxidation rates that were calculated from Stations 52 (0.11 nM/h) and 60 (4.9 nM/h), respectively (see section 3.3), and estimate the pMn(III/IV) formed at night by multiplying the length of night at each station by the Mn oxidation rates (Table S1). To estimate the upper bound of AOS at dawn (hereafter the AOS_{dawn}), we use the measured pMn(II) at time of sampling and assume it is constant throughout the day-night cycle and the estimated pMn(III/IV) produced during nighttime oxidation as pMn(IV) to calculate AOS_{dawn} (Figure 4b).

The similar measured AOS at Stations 57 (2.37) and 43 (2.34) belies the different processes at work at these two basin stations: Station 57 had a longer night and thus higher estimated AOS_{dawn}, but it also had higher integrated shortwave radiation by the time of sampling (1.42×10^6 vs. 2.06×10^5 J/m^2), which decreased the AOS greatly (Figure 4a). Station 48 has the

highest measured AOS (3.11) as a result of the high estimated AOS_{dawn} (3.65) and the lowest integrated shortwave radiation (1.44×10^5 J/m^2). Fully ice-covered basin Stations 19-38 were sampled under 24-hour light conditions. Extended exposure to light (>3000 hours) inhibits oxidation, resulting in low measured AOS (median=2.10) (Figure 2b).

At relatively warm and nutrient-rich shelf stations, higher Mn dark oxidation rates lead to higher estimated AOS (~4) at dawn compared to cold and oligotrophic basin stations (Figure 4b). At Stations 6 and 66, a high magnitude of integrated shortwave radiation (9.21×10^6 and 2.22×10^6 J/m^2, respectively) leads to low measured AOS at the time of sampling (2.03 and 2.11, respectively). It is puzzling, however, to observe low measured AOS (2.11) at Station 61, despite having a high estimated AOS_{dawn} (3.88) and low integrated shortwave radiation (2.35×10^5 J/m^2) (Figure 4a). Similar to the faster oxidation rate at slope Station 60 compared to basin Station 52, factors such as temperature and microbial communities may also lead to higher light-dependent Mn reduction rates at the shelf stations compared to basin stations. Alternatively, given the high concentrations of humic substances in the Chukchi Sea (Hioki et al., 2014; Nakayama et al., 2011), it is possible that Mn oxidation at night was inhibited at shelf stations (6, 61, 66) due to strong dissolved Mn(III)-ligand complexes (Oldham et al., 2021). However, the inhibition of Mn oxidation cannot be a universal phenomenon in the Chukchi Sea, since slope Station 60 has a high AOS.

4 Conclusions

The observed relationship between the pMn AOS and SZA demonstrates the significance of light in the Mn redox cycling in the Western Arctic Ocean. Such a relationship could also

312 exist in other regions globally, but similar synchrotron-based analyses are more challenging due
313 to much lower pMn concentrations compared to the surface Arctic Ocean.

314 We estimated that the Mn oxidation rate at night in the surface oligotrophic Arctic basins
315 during our cruise is ~0.1 nM/h. Such rates of Mn oxidation take place even within the near-
316 freezing (~-1.5 ˚C) Polar Mixed Layer in late summer. This study serves as the first study to
317 infer in-situ Mn oxidation at such cold temperatures. The oxidation of dissolved Mn(II) in the
318 extended polar winter with no sunlight could serve as a significant seasonal Mn removal
319 mechanism out of the surface layer. Assuming that the Mn oxidation rate remains at 0.1 nM/h in
320 the Arctic winter when it is dark 24 hrs a day, and that riverine and benthic sources of dissolved
321 Mn diminish in winter, it would only take ~50 hours (~2 days) to oxidize the entire reservoir of
322 dissolved Mn in the surface Western Arctic Ocean (~5 nM; Jensen et al., 2020) and then sink out
323 of the Polar Mixed Layer. To our knowledge, no measurements of dissolved or particulate Mn
324 exist in the Arctic winter to test this prediction.

325 To date, rapid redox cycles of Mn during the day-night cycle have been observed in the
326 Western Arctic Ocean (this study) and coastal North Atlantic Ocean (Oldham et al., 2020; Sunda
327 & Huntsman, 1990). In contrast, Mn oxidation is absent in the surface Sargasso Sea throughout
328 the day and night, whereas it is present in the dark subsurface (Sunda & Huntsman, 1988).
329 Oldham et al. (2021) did not detect particulate Mn(IV) formation in either sun-lit surface or dark
330 subsurface waters in the Ross Sea. The conditions that govern the diel Mn redox cycle are not
331 clear, but have important implications for availability of Mn and other pMn-associated
332 micronutrients such as cobalt (Oldham et al., 2021). Future work is needed to investigate the
333 relative importance of light levels, Mn(III)-ligand complexes, microbial communities, and/or

reactive oxygen species in controlling Mn redox cycling and its impacts on biogeochemical cycles of different particle-reactive elements.

Acknowledgments, Samples, and Data

This work was supported by the Chemical Oceanography program through the National Science Foundation under grant number NSFOCE-1535854 to PJL. This research was carried out at the Stanford Synchrotron Radiation Lightsource, supported by the U.S. Department of Energy, Office of Science, Office of Basic Energy Sciences under Contract No. DE-AC02-76SF00515. We would like to thank all scientists and crew on board the USCGC icebreaker Healy during the GN01 Arctic GEOTRACES cruise. We thank co-chief scientist William Landing from Florida State University for providing underway shortwave radiation data, and Susan Becker from the Oceanographic Data Facility (ODF) at Scripps Institution of Oceanography for providing photosynthetically available radiation data. The ODF hydrographic, PAR, and pH data are available on the Biological and Chemical Oceanography Data Management Office (BCO-DMO) (https://www.bco-dmo.org/dataset/700817 and https://www.bco-dmo.org/dataset/646825). The conversion between voltage and $\mu E/m^2/s$ in PAR data is based on the calibration conducted before the cruise. Particulate Mn data collected by in-situ pumps in the GN01 cruise are available on the BCO-DMO (https://www.bco-dmo.org/dataset/807340). Many thanks to Ryan C. Davis for the support at the Beamline 11-2, Carl Lamborg and Colleen Hansel for insights in the discussion, Colleen Hansel for providing XANES reference spectra including δ-MnO_2 and feitknechtite, Jena E. Johnson for Mn silicates reference spectra, Peter Kopittke for Mn citrate and oxalate reference spectra, and Hudson Carvalho for Mn-EDTA reference spectra.

References

Blamey, F. P. C., McKenna, B. A., Li, C., Cheng, M., Tang, C., Jiang, H., et al. (2018). Manganese distribution and speciation help to explain the effects of silicate and phosphate on manganese toxicity in four crop species. *New Phytologist*, *217*(3), 1146-1160. https://doi.org/10.1111/nph.14878

Browning, T. J., Achterberg, E. P., Engel, A., & Mawji, E. (2021). Manganese co-limitation of phytoplankton growth and major nutrient drawdown in the Southern Ocean. *Nature Communications*, *12*(1), 884. https://doi.org/10.1038/s41467-021-21122-6

Carroll, S., O'Day, P. A., Esser, B., & Randall, S. (2002). Speciation and fate of trace metals in estuarine sediments under reduced and oxidized conditions, Seaplane Lagoon, Alameda Naval Air Station (USA). *Geochemical Transactions*, *3*(10), 81-101. https://doi.org/10.1039/B205002A

Charette, M. A., Kipp, L. E., Jensen, L. T., Dabrowski, J. S., Whitmore, L. M., Fitzsimmons, J. N., et al. (2020). The Transpolar Drift as a source of riverine and shelf-derived trace elements to the central Arctic Ocean. *Journal of Geophysical Research: Oceans*, *125*(5). https://doi.org/10.1029/2019jc015920

Clement, B. G., Luther, G. W., & Tebo, B. M. (2009). Rapid, oxygen-dependent microbial Mn(II) oxidation kinetics at sub-micromolar oxygen concentrations in the Black Sea suboxic zone. *Geochimica et Cosmochimica Acta*, *73*(7), 1878-1889. https://doi.org/10.1016/j.gca.2008.12.023

Colombo, M., Jackson, S. L., Cullen, J. T., & Orians, K. J. (2020). Dissolved iron and manganese in the Canadian Arctic Ocean: On the biogeochemical processes controlling their distributions. *Geochimica et Cosmochimica Acta*, *277*, 150-174. https://doi.org/10.1016/j.gca.2020.03.012

Dick, G. J., Clement, B. G., Webb, S. M., Fodrie, F. J., Bargar, J. R., & Tebo, B. M. (2009). Enzymatic microbial Mn(II) oxidation and Mn biooxide production in the Guaymas Basin deep-sea hydrothermal plume. *Geochimica et Cosmochimica Acta*, *73*(21), 6517-6530. https://doi.org/10.1016/j.gca.2009.07.039

Goldberg, E. D. (1954). Marine Geochemistry 1. Chemical Scavengers of the Sea. *The Journal of Geology*, *62*(3), 249-265

Gunter, K. K., Aschner, M., Miller, L. M., Eliseev, R., Salter, J., Anderson, K., & Gunter, T. E. (2006). Determining the oxidation states of manganese in NT2 cells and cultured astrocytes. *Neurobiology of Aging*, *27*(12), 1816-1826. https://doi.org/10.1016/j.neurobiolaging.2005.10.003

Hansel, C. M., & Francis, C. A. (2006). Coupled photochemical and enzymatic Mn(II) oxidation pathways of a planktonic *Roseobacter*-like bacterium. *Applied and Environmental Microbiology*, *72*(5), 3543. https://doi.org/10.1128/AEM.72.5.3543-3549.2006

Harrington, J. M., Parker, D. L., Bargar, J. R., Jarzecki, A. A., Tebo, B. M., Sposito, G., & Duckworth, O. W. (2012). Structural dependence of Mn complexation by siderophores: Donor group dependence on complex stability and reactivity. *Geochimica et Cosmochimica Acta*, *88*, 106-119. https://doi.org/10.1016/j.gca.2012.04.006

Hermans, M., Lenstra, W. K., van Helmond, N. A. G. M., Behrends, T., Egger, M., Séguret, M. J. M., et al. (2019). Impact of natural re-oxygenation on the sediment dynamics of manganese, iron and phosphorus in a euxinic Baltic Sea basin. *Geochimica et Cosmochimica Acta*, *246*, 174-196. https://doi.org/10.1016/j.gca.2018.11.033

Hioki, N., Kuma, K., Morita, Y., Sasayama, R., Ooki, A., Kondo, Y., et al. (2014). Laterally spreading iron, humic-like dissolved organic matter and nutrients in cold, dense subsurface water of the Arctic Ocean. *Scientific Reports*, *4*, 6775. https://doi.org/10.1038/srep06775

Jensen, L. T., Morton, P. L., Twining, B. S., Heller, M. I., Hatta, M., Measures, C. I., et al. (2020). A comparison of marine Fe and Mn cycling: U.S. GEOTRACES GN01 Western Arctic case study. *Geochimica et Cosmochimica Acta*, *288*, 138-160. https://doi.org/10.1016/j.gca.2020.08.006

Kim, K., Yoon, H. I., & Choi, W. (2012). Enhanced dissolution of manganese oxide in ice compared to aqueous phase under illuminated and dark conditions. *Environmental Science & Technology*, *46*(24), 13160-13166. https://doi.org/10.1021/es302003z

Kipp, L. E., Charette, M. A., Moore, W. S., Henderson, P. B., & Rigor, I. G. (2018). Increased fluxes of shelf-derived materials to the central Arctic Ocean. *Science advances*, *4*(1), eaao1302. https://doi.org/10.1126/sciadv.aao1302

Landing, W. M., Cutter, G., & Kadko, D. C. (2017). CTD-ODF profiles from GEOTRACES-Arctic Section cruise HLY1502, August to October 2015 (U.S. GEOTRACES Arctic project). *Biological and Chemical Oceanography Data Management Office (BCO-DMO), Dataset version 2017-05-22*. Retrieved from http://lod.bco-dmo.org/id/dataset/700817

Learman, D. R., Wankel, S. D., Webb, S. M., Martinez, N., Madden, A. S., & Hansel, C. M. (2011). Coupled biotic–abiotic Mn(II) oxidation pathway mediates the formation and structural evolution of biogenic Mn oxides. *Geochimica et Cosmochimica Acta*, *75*(20), 6048-6063. https://doi.org/10.1016/j.gca.2011.07.026

Lee, J., Kang, S. H., Yang, E. J., Macdonald, A. M., Joo, H. M., Park, J., et al. (2019). Latitudinal distributions and controls of bacterial community composition during the

summer of 2017 in Western Arctic Surface waters (from the Bering Strait to the Chukchi Borderland). *Scientific Reports*, *9*(1), 16822. https://doi.org/10.1038/s41598-019-53427-4

Lee, J. M., Lam, P. J., Vivancos, S. M., Pavia, F. J., Anderson, R. F., Lu, Y., et al. (2021). Changing chemistry of particulate manganese in the near- and far-field hydrothermal plumes from 15°S East Pacific Rise and its influence on metal scavenging. *Geochimica et Cosmochimica Acta*, *300*, 95-118. https://doi.org/10.1016/j.gca.2021.02.020

Lee, Z., Hu, C., Shang, S., Du, K., Lewis, M., Arnone, R., & Brewin, R. (2013). Penetration of UV-visible solar radiation in the global oceans: Insights from ocean color remote sensing. *Journal of Geophysical Research: Oceans*, *118*(9), 4241-4255. https://doi.org/10.1002/jgrc.20308

Lenz, C., Behrends, T., Jilbert, T., Silveira, M., & Slomp, C. P. (2014). Redox-dependent changes in manganese speciation in Baltic Sea sediments from the Holocene Thermal Maximum: An EXAFS, XANES and LA-ICP-MS study. *Chemical Geology*, *370*, 49-57. https://doi.org/10.1016/j.chemgeo.2014.01.013

Luther, G. W. (2005). Manganese(II) oxidation and Mn(IV) reduction in the environment—two one-electron transfer steps versus a single two-electron step. *Geomicrobiology Journal*, *22*(3-4), 195-203. https://doi.org/10.1080/01490450590946022

Machado, B. A., Gomes, M. H. F., Marques, J. P. R., Otto, R., & de Carvalho, H. W. P. (2019). X-ray spectroscopy fostering the understanding of foliar uptake and transport of Mn by soybean (*Glycine max* L. Merril): Kinetics, chemical speciation, and effects of glyphosate. *Journal of Agricultural and Food Chemistry*, *67*(47), 13010-13020. https://doi.org/10.1021/acs.jafc.9b05630

Middag, R., de Baar, H. J. W., Klunder, M. B., & Laan, P. (2013). Fluxes of dissolved aluminum and manganese to the Weddell Sea and indications for manganese co-limitation. *Limnology and Oceanography*, *58*(1), 287-300. https://doi.org/10.4319/lo.2013.58.1.0287

Middag, R., de Baar, H. J. W., Laan, P., & Klunder, M. B. (2011). Fluvial and hydrothermal input of manganese into the Arctic Ocean. *Geochimica et Cosmochimica Acta*, *75*(9), 2393-2408. https://doi.org/10.1016/j.gca.2011.02.011

Nakayama, Y., Fujita, S., Kuma, K., & Shimada, K. (2011). Iron and humic-type fluorescent dissolved organic matter in the Chukchi Sea and Canada Basin of the western Arctic Ocean. *Journal of Geophysical Research: Oceans*, *116*(C7). https://doi.org/10.1029/2010jc006779

Newville, M. (2001). IFEFFIT: Interactive XAFS analysis and FEFF fitting. *Journal of Synchrotron Radiation*, *8*(2), 322-324. https://doi.org/10.1107/S0909049500016964

Nico, P. S., Anastasio, C., & Zasoski, R. J. (2002). Rapid photo-oxidation of Mn(II) mediated by humic substances. *Geochimica et Cosmochimica Acta*, *66*(23), 4047-4056. https://doi.org/10.1016/S0016-7037(02)01001-3

Oldham, V. E., Chmiel, R., Hansel, C. M., DiTullio, G. R., Rao, D., & Saito, M. A. (2021). Inhibited manganese oxide formation hinders cobalt scavenging in the Ross Sea. *Global Biogeochemical Cycles*, *n/a*(n/a), e2020GB006706. https://doi.org/10.1029/2020GB006706

Oldham, V. E., Lamborg, C. H., & Hansel, C. M. (2020). The spatial and temporal variability of Mn speciation in the coastal Northwest Atlantic Ocean. *Journal of Geophysical Research: Oceans*, *125*(1), e2019JC015167. https://doi.org/10.1029/2019JC015167

Peers, G., & Price, N. M. (2004). A role for manganese in superoxide dismutases and growth of iron-deficient diatoms. *Limnology and Oceanography*, *49*(5), 1774-1783. https://doi.org/10.4319/lo.2004.49.5.1774

Sunda, W. G., & Huntsman, S. A. (1987). Microbial oxidation of manganese in a North Carolina estuary1. *Limnology and Oceanography*, *32*(3), 552-564. https://doi.org/10.4319/lo.1987.32.3.0552

Sunda, W. G., & Huntsman, S. A. (1988). Effect of sunlight on redox cycles of manganese in the southwestern Sargasso Sea. *Deep Sea Research Part A. Oceanographic Research Papers*, *35*(8), 1297-1317. https://doi.org/10.1016/0198-0149(88)90084-2

Sunda, W. G., & Huntsman, S. A. (1990). Diel cycles in microbial manganese oxidation and manganese redox speciation in coastal waters of the Bahama Islands. *Limnology and Oceanography*, *35*(2), 325-338. https://doi.org/10.4319/lo.1990.35.2.0325

Sunda, W. G., & Huntsman, S. A. (1994). Photoreduction of manganese oxides in seawater *Marine Chemistry*, *46*, 133-152. https://doi.org/10.1016/0304-4203(94)90051-5

Sunda, W. G., Huntsman, S. A., & Harvey, G. R. (1983). Photoreduction of manganese oxides in seawater and its geochemical and biological implications. *Nature*, *301*(5897), 234. https://doi.org/10.1038/301234a0

Tebo, B. M., Bargar, J. R., Clement, B. G., Dick, G. J., Murray, K. J., Parker, D., et al. (2004). Biogenic manganese oxides: Properties and mechanisms of formation. *Annual Review of Earth and Planetary Sciences*, *32*(1), 287-328. https://doi.org/10.1146/annurev.earth.32.101802.120213

Toyoda, K., & Tebo, B. M. (2016). Kinetics of Mn(II) oxidation by spores of the marine Bacillus sp. SG-1. *Geochimica et Cosmochimica Acta*, *189*, 58-69. https://doi.org/10.1016/j.gca.2016.05.036

van Hulten, M., Middag, R., Dutay, J. C., de Baar, H., Roy-Barman, M., Gehlen, M., et al. (2017). Manganese in the west Atlantic Ocean in the context of the first global ocean

493 circulation model of manganese. *Biogeosciences*, *14*(5), 1123-1152.
494 https://doi.org/10.5194/bg-14-1123-2017
495 Von Langen, P. J., Johnson, K. S., Coale, K. H., & Elrod, V. A. (1997). Oxidation kinetics of
496 manganese (II) in seawater at nanomolar concentrations. *Geochimica et Cosmochimica Acta*,
497 *61*(23), 4945-4954. https://doi.org/10.1016/S0016-7037(97)00355-4
498 Webb, S. M. (2005). SIXPack a graphical user interface for XAS analysis using IFEFFIT.
499 *Physica Scripta*, 1011. https://doi.org/10.1238/physica.topical.115a01011
500 Woosley, R. J., Millero, F. J., & Takahashi, T. (2017). Internal consistency of the inorganic
501 carbon system in the Arctic Ocean. *Limnology and Oceanography: Methods*, *15*(10), 887-
502 896. https://doi.org/10.1002/lom3.10208
503 Xiang, Y., & Lam, P. J. (2020). Size-fractionated compositions of marine suspended particles in
504 the Western Arctic Ocean: Lateral and vertical sources. *Journal of Geophysical Research:*
505 *Oceans*, *125*(8), e2020JC016144. https://doi.org/10.1029/2020JC016144
506 Yano, J., Kern, J., Sauer, K., Latimer, M. J., Pushkar, Y., Biesiadka, J., et al. (2006). Where
507 water is oxidized to dioxygen: Structure of the photosynthetic Mn4Ca cluster. *Science*,
508 *314*(5800), 821-825. https://doi.org/10.1126/science.1128186
509